AUT Journal of Civil Engineering

AUT J. Civil Eng., 2(2) (2018) 161-176
DOI: 10.22060/ajce.2018.14611.5487

Exterior Concrete Beam-column Connection Reinforced with Glass Fiber Reinforced Polymers (GFRP) bars under CyclicL loading

H. Rezaee Azariani, H. Shariatmadar*, M. Reza Esfahani

Department of Civil Engineering, Ferdowsi University of Mashhad, Mashhad, Iran.

ABSTRACT: This paper is devoted to assess the behavior of the exterior concrete beam-column connections reinforced with Glass Fiber Reinforced Polymers (GFRP) bars under cyclic loading. For this purpose, 8 different beam-column connections were experimentally investigated. In these specimens, concrete with compressive strength of 30 and 45 MPa was employed. In four of these connections, GFRP bars were used while the others were reinforced with steel bars. The confinement of longitudinal bars was different in the connections. The GFRP-reinforced beam-column connection showed an elastic behavior with very low plasticity features under cyclic loading. This resulted in lower energy dissipation compared to the steel-reinforced beam-column connections. The GFRP-reinforced beam-column connections showed lower stiffness than that of the steel-reinforced beam-column connections. Load-story drift envelope for specimens with GFRP bars showed an acceptable drift capacity. These specimens had the essential requirements for acting as a member of a moment frame in seismic regions. In case of GFRP strengthened specimens with low and high strength concrete, increasing the cyclic loading results in flexural failure of the beam in the beam-column connection region. Increasing the confinement of concrete beams leads to the reduction of crack width. Furthermore, at higher drifts, spalling was not observed in concrete surface in beam-column connection region. In the analytical parts of the study, specimens were simulated using the SeismoStruct software. Experimental and analytical results showed a satisfactory correlation.

Review History:

Received: 17 June 2018
Revised: 27 July 2018
Accepted: 16 December 2018
Available Online: 11 August 2018

Keywords:

Glass Fiber Reinforced Polymers (GFRP)
Reinforced Concrete
Beam-Column connection
cyclic Loading

1- Introduction

According to field observations of damages in reinforced concrete (RC) buildings caused by earthquakes, it was proved that these damages usually occurred in beam-column connection parts of the buildings. Consequently, Park and Paulay [1] comprehensively studied the behavior of beam-column connections. They concluded that the crucial zone of the connection is its panel zone and suggested to modify its design procedure.

Low bonding resistance and shear fracture in connection zone may lead to slippage between the concrete and the reinforcing steel bars. This phenomenon was investigated by Paulay and Priestley [2]. Based on their work, the panel zone, whose beams and columns are designed without controlling the stress induced in the connection, is weak. These connections are required to be redesigned. By conducting various tests on specimens made of high-strength concrete.

Recently, self-consolidating concrete has been widely used due to its high workability for casting heavily reinforced sections. This type of concrete does not require any vibrator. Hence, it can be utilized in areas with congested reinforcement such as connection zones and columns. Said [3] experimentally assessed the behavior of connections made with low concrete and self-consolidating concrete. The shear deformations of these connections were similar, but, in large deformations, load-carrying capacity of the connections made of self-consolidating concrete was more than that of the low ones. This is because of the fact that the aggregates of the self-consolidating concrete are finer relative to the low concrete. Kang et al. [4] assessed the effects of head size, shape and head-attaching technique on the behavior of the exterior connections. Based on the fracture mechanics, Barbhuiya and Choudhury [5] studied the size effect of RC beam-column connections under cyclic loading. Furthermore, Engindeniz et al. [6] assessed the behavior of beam-column concrete connections under lateral loadings.

In the past few decades, composite materials have been extensively applied in repairing and strengthening of RC structures. Fiber reinforced polymer (FRP) is one the well-known composite materials used in strengthening the RC buildings. Nowadays, FRP bars are produced and utilized in concrete members. They are made of resin and fiber instead of steel. Similarly, two polymer components, including the FRP and resin form the composite FRP bars. They can be made of carbon, glass or Aramid. Accordingly, three different bars, namely glass fiber-reinforced polymer (GFRP), carbon fiber-reinforced polymer (CFRP) and aramid fiber-reinforced polymer (AFRP) bars are available [7]. Said and Nehdi [8] reflected that the main concern about the usage of FRP bar

Corresponding author, E-mail: shariatmadar@um.ac.ir

was their low ductility and energy dissipation capacity.

Additionally, Toutanji and Saafi [9], Salib and Abdel-Sayed [10] suggested the application of FRP bars for concrete buildings due to their high corrosion resistance. Vijay [11] dealt with the aging of the concrete members reinforced with GFRP bars, and studied the effects of ultimate strength and stiffness on the fracture modes. Zou [12-, 13, 14] conducted vast researches on Long-term deflection and cracking behavior of concrete beams prestressed with CFRP. Alsayed et al. [15] investigated the behavior of the short columns reinforced with GFRP vertical stirrups. They observed that usage of these stirrups led to reduction in axial load carrying capacity of columns. Furthermore, Grira and Saatcioglu [16] compared the performance of CFRP bars and transverse bars in columns.

Then, Shehata [17], Nagasaka et al. [18], Sugita [19] suggested FRP bars for using in concrete structures due to their light weight, high durability and being non-magnetic. Besides, Ahmed et al. [20] and Benmokrane et al. [21] believed that usage of FRP bars in concrete bridges provided environmental and economic benefits. Additionally, Mohamed and Benmokrane [22] suggested using GFRP bars with high elasticity modulus as the main bars of the foundation, walls and the roof slab of the concrete tanks. It should be reminded that FRP grids are widely applied in concrete decks, curtain walls, water tanks, slabs and lining of the underground tunnels because of advantages such as suppression of delamination [23]. Afterwards, Lemaitre and Desmorat [24] assessed the damage index of the connections reinforced with FRP bars. Corley [25] highlighted that the concrete connections reinforced with FRP bars had enough ductility.

Sabzi and Esfahani [26] studied the effect of arrangement of reinforcement on the concrete cover separation in strengthened RC beams. Twelve beams were cast and evaluated through four-point bending test. The specimens with low and medium ratios of reinforcement, having small-diameter bars, were provided a higher load capacity and sustained more deflection before FRP debonding. Aiello and Ombres [27] experimentally investigated beams reinforced with hybrid steel-FRP bars and beams reinforced with FRP bars. The findings proved that the hybrid beams were more ductile than the beams reinforced with FRP bars. Additionally, utilizing hybrid steel-FRP bars led to more reduction in the beam deflection, in comparison to the usage of FRP bars. Leung and Balendran [28] used hybrid bars in concrete beams to avoid ductility reduction.

Alcocer et al. [29] tested two full-scale beam-column connections in a precast concrete frame under uni-directional and bi-directional cyclic loading which simulated ground motions during earthquake. It should be mentioned that bending of bars reduces their strength. Usage of FRP grids composed of new fiber composite material for reinforcing concrete can remedy this problem. Beydokhty and Shariatmadar [30] carried out an investigation on the mechanical properties of repaired beam-column connections tested under reverse cyclic loading. Based on the responses of the tested specimens it was demonstrated that the externally bonded retrofitting method using CFRP sheets was suitable for rehabilitating the seismic capacity of the connections. This technique provided a considerable enhancement in energy dissipation and the performance. Furthermore, it resulted in improved type of damages relative to the modes of damages for the specimens in the process of initial loading. Bossio et al. [31] conducted a research with the purpose of exploring the seismic behavior as well as the failure modes of T-shaped beam-column connections in RC elements. An analytical model for connection behavior was proposed, and accordingly theoretical simulations were performed. The results obtained from the experimental program were reported and then compared with the predictions acquired based on the proposed model.

This paper has been conducted with the intent of comparing the exterior beam-column connections reinforced with GFRP bars and with steel bars. In this process, the low and high-strength concrete have been utilized. Additionally, considering different confinements due to the transverse reinforcement and detailing, the behavior of the GFRP bars have been compared with the steel bars.

2- Test program

2- 1- Description of specimen

A beam-column connection specimen is a part of a frame and made by cutting through a beam's points of contra-flexure on both sides of the column and cutting through the column one-half story height above and below the connection as shown in Figure. 1. Note that; the points of contra-flexure do not always lie at the mid-points of beams and columns, and their position may be changed due to the existence of the dynamic forces. Nevertheless, the effect of their transformation on the connection core can be ignored because of the fact that these changes in position are negligible [5]. In this work, several concrete external beam-column connections of a two-dimensional frame have been tested. The height and span of this frame are equal to 4 m and 3.6 m, respectively, and the section of the connection is a 200×200 mm^2. It should be noted that one-half scaled specimens were adopted. The connection detailing, its free diagram and geometrical properties are shown in Figure. 1.

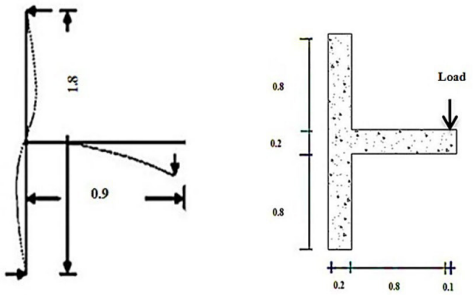

(a) Free body diagram of the connection (b)The geometrical properties (m)

Figure 1. Detailing of the exterior beam-column connection

In this study, 8 different exterior concrete beam-column connections were constructed and tested. Four of these connections are reinforced with the fiber reinforced polymer bar while the others are reinforced with the steel bars. The GFRP bars were used in the aforesaid specimens. Two types of concrete including the low and high strength (self-consolidating) concrete were employed for casting the specimens. The self-consolidating concrete was utilized because of its high-strength and workability. In Table 1, the

detailing of the specimens and the abbreviated names of the steel and GFRP bars are listed. Row 1 to 4 in this table belongs to the specimens reinforced with steel bars, and row 5 to 8 is related to the specimens with GFRP bars.

Table 1. Detailing of the specimen and the abbreviated names of the steel and FRP bars

Specimens	Names
1	CONF_STEEL_C30
2	UNCONF_STEEL_C30
3	CONF_STEEL_C45
4	UNCONF_STEEL_C45
5	CONF_GFRP_C30
6	UNCONF_GFRP_C30
7	CONF_GFRP_C45
8	UNCONF_GFRP_C45

Figure 2 is associated with the specimens reinforced with steel bars, and Figure 3 is related to the specimens with GFRP bars. CONF represents the confinement of the connection and indicates that the stirrups with spacing of 75 mm are placed in the beams and columns at their faces and extend 2d [32]. UNCONF represents the unconfined connection in which the stirrups are applied at spacing of 150 mm. Moreover, "steel" and "GFRP" represents usage of steel and GFRP bars, respectively. Additionally, the low and self-consolidating concrete with cylindrical compressive strength of 30 and 45 MPa are presented by C30 and C45, respectively. The detailing of specimens including the reinforcement arrangement, bar size, the space between bars and their sections are presented in Figure 2 for the specimens reinforced with steel bars. In Figure 3, the aforementioned parameters are presented for the specimens with GFRP bars. Moreover, the geometrical properties of the specimens are illustrated in Table 2.

2- 2- Material Properties

In the specimens, deformed steel bar A3 were used. The diameter of the longitudinal and transverse deformed bars of the specimens was 8 mm and 14 mm, respectively. In this work, deformed glass fiber reinforced polymer bars with diameter of 14 mm (for longitudinal bars of the beam) were employed. To prevent the GFRP bars from sliding from the mechanical couplers, Memo Hot glue with the length of 50 cm was utilized. In this research, the mechanical properties of the bars were determined with the help of tensile test setup. The specimen utilized in this test is presented in Figure 4. The specimens with GFRP bars are shown in Figures 5 and 6 illustrates the details of the mechanical couplers with the GFRP before molding, and the GFRP bars with the mechanical couplers are shown. In Figure 7 demonstrates the stress-strain curve of the steel and GFRP bars.

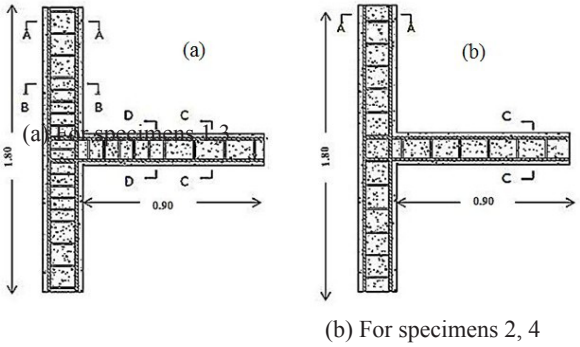

(b) For specimens 2, 4

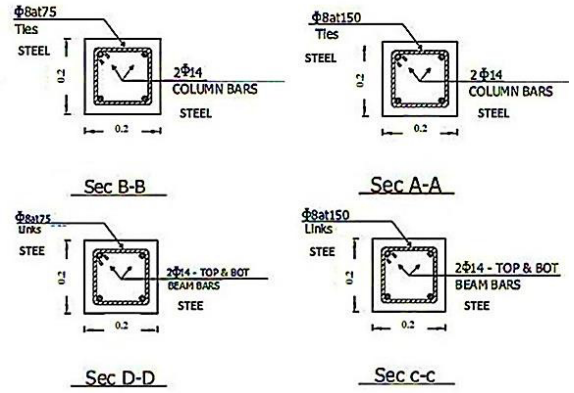

Figure 2. The specimens of the exterior connection reinforced with steel (dimensions are in terms of meter)

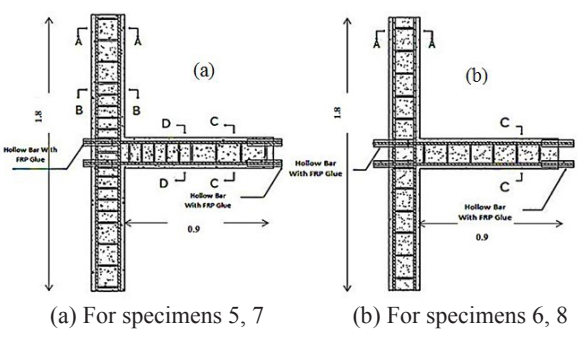

(a) For specimens 5, 7 (b) For specimens 6, 8

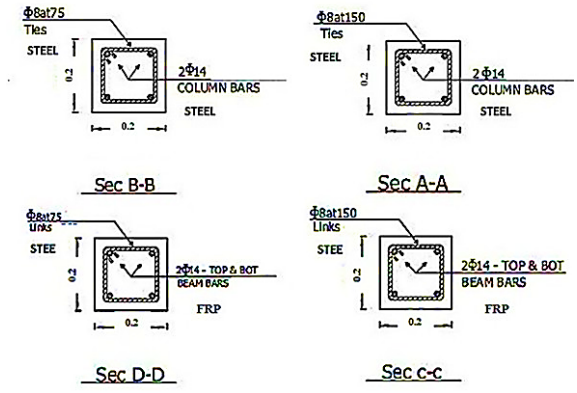

Figure 3. The specimens of the exterior connection reinforced with GFRP (dimensions are in terms of meter)

Table 2. Details of materials and geometry of specimens

Specimens	steel		GFRP	
	1,3 (CONF_TEEL_C30) (CONF_STEEL_C45)	2,4 (UNCONF_STEEL_C30) (UNCONF_STEEL_C45)	5,7 (CONF_GFRP_C30) (CONF_GFRP_C45)	6,8 (UNCONF_GFRP_C30) (UNCONF_GFRP_C45)
Beam Dimension (mm)	200 × 200	200 × 200	200 × 200	200 × 200
Longitudinal reinforcement (T&B)	4Φ14- steel	4Φ14- steel	4Φ14- GFRP	4Φ14- GFRP
Transverse reinforcement Column	Φ8 @75-150 (steel)	Φ8 @150 (steel)	Φ8 @75-150 (steel)	Φ8 @150 (steel)
Dimension (mm)	200 × 200	200 × 200	200 × 200	200 × 200
Longitudinal reinforcement	4Φ14- steel	4Φ14- steel	4Φ14- steel	4Φ14- steel
Transverse reinforcement Column	Φ8 @75-150 (steel)	Φ8 @150 (steel)	Φ8 @75-150 (steel)	Φ8 @150 (steel)

Figure 4. GFRP bar specimen used in tensile test

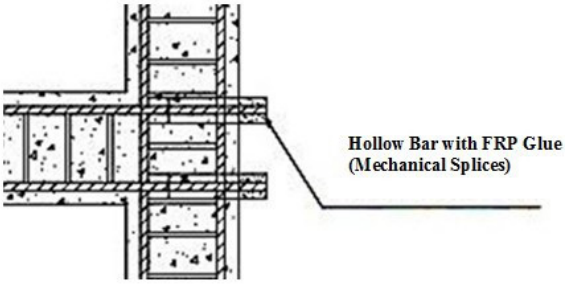

Figure 5. The details of mechanical coupler with GFRP bars

Figure 6. GPRF bars with mechanical couplers before molding

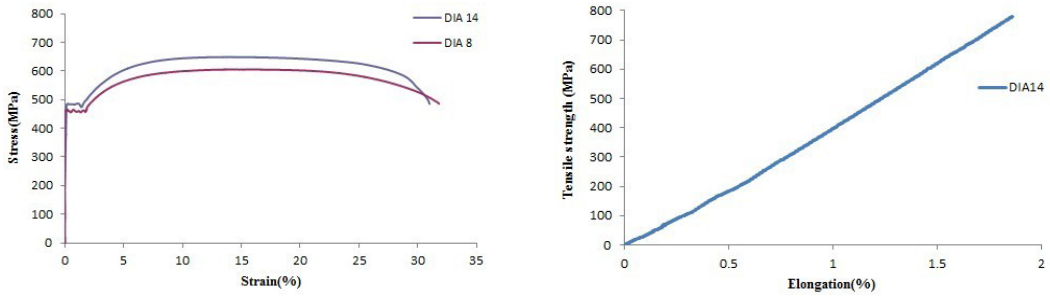

(a) steel bars (b) GFRP bars

Figure 7. Stress-strain curve of the bars

Due to the fact that two types of concrete with different strength were studied in this research, casting the specimens was done in two steps. In each step, four cylindrical specimens were made. Compressive test was conducted on these samples and the connections simultaneously. In each sampling, the average of the compressive strength of the cylindrical specimens was measured, and it was assumed that the specified concrete strength of the connection was equal to the obtained value. Moreover, in Table 3, the properties of the materials of the specimens are listed.

Table 3. The properties of the materials of the specimens are listed

Specimens	steel		GFRP	
	1,2 CONF_STEEL_C30 UNCONF_STEEL_C30	3,4 CONF_STEEL_C45 UNCONF_STEEL_C45	5,6 CONF_FRP_C30 UNCONF_FRP_C30	7,8 CONF_FRP_C45 UNCONF_FRP_C45
Concrete	NC	SCC	NC	SCC
Compressive	30.1	45.4	30.1	45.4
Strength (MPa)				
steel (longitudinal)				
Yield strength (MPa)	484	484	550	550
Ultimate strength (MPa)	649	649	1100	1100
Young's Modulus (GPa)	202.4	202.4	83	83
Stirrups (transverse)				
Yield strength (MPa)	463	463	463	463
Ultimate strength (MPa)	605	605	605	605
Young's modulus (GPa)	202.4	202.4	202.4	202.4
GFRP				
Tensile strength (MPa)	-	-	800	800
Tensile modulus (GPa)	-	-	43	43
Specific weight (N/mm^3)	-	-	1.8E-5	1.8E-5

2- 3- Test setup

To apply cyclic load at the end of the beam, a hydraulic jack of 600 kN capacity was utilized. In order to measure the applied force, a load cell with the capacity of 200 kN was adopted. As shown in Figure. 8, steel plates were installed on the beam and column ends for preventing the lateral displacements and maintaining the equilibrium in the specimens.

It should be mentioned that the first LVDT connected to a personal computer (PC) measured the vertical displacement of the beam end. Besides, in order to measure the vertical displacement of the connection at the distance of 2h [32], the LVDT2 was installed on the beam. This LVDT was connected to the PC and recorded the vertical displacement of the beam Δ_2 in the critical zone. Additionally, the LVDT5 was installed on the beam for measuring the vertical displacement of the connection, and the LVDT3 and LVDT4 were placed on the column to find the rotation of the connection. It should be reminded that the LVDTs 3, 4 and 5 measured displacements Δ_3, Δ_4 and Δ_5, respectively. Note that; LVDT5 was installed on the connection core and LVDT3 and LVDT4 were placed in the column. The test setup and LVDTs and the details of the LVDTs at the connection are shown in Figures. 8 and Fig. 9, respectively.

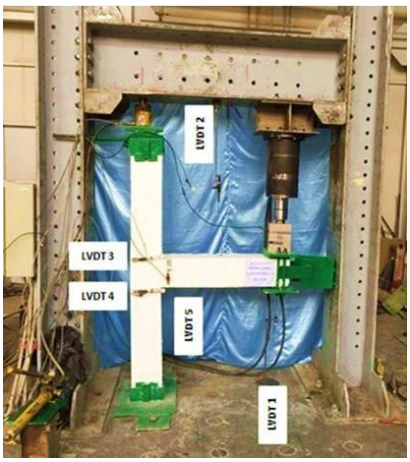

Figure 8. The test setup and LVDTs

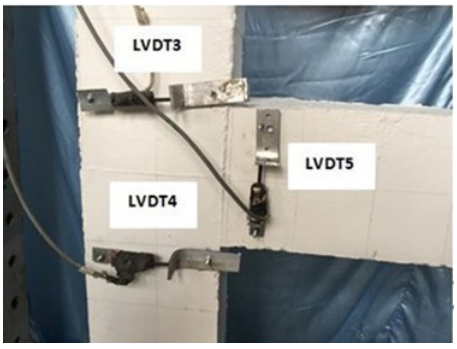

Figure 9. The details of the LVDTs at the connection

The displacement-controlled cyclic load was applied to the specimens. The drift applied to the beam was calculated based on the lateral displacement of the beam-column connection and the obtained results are shown in Figure 10.

Figures 10a and b illustrate the deformation of the actual exterior beam-column connection of a multi-story moment resisting frame and the corresponding deformation of the experimental model, respectively. Note that; θ denotes the angle of the inter-story drift obtained by dividing δ (drift) by H (column height). When the beam can freely rotate, θ can be calculated using the vertical displacement of the beam end.

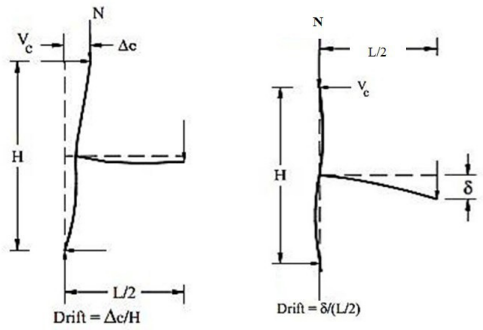

(a) Actual structure (b) Experimental specimen

Figure 10. Calculation of the beam end's drift (m)

To simulate the earthquake force, the cyclic loading shown in Figure. 11 was used. The loading included two steps. In the first step, the force-controlled force was applied until the specimen cracked. In this step, the specimen behavior was linear. Then, the displacement-controlled force was applied to the specimen until reaching the 5% drift. In this test, the column was subjected to the axial force equal to $0.10f_c' A_g$. In each loading cycle, the value of this force was monitored to modify if the force value was reduced due to the deformation of the specimen.

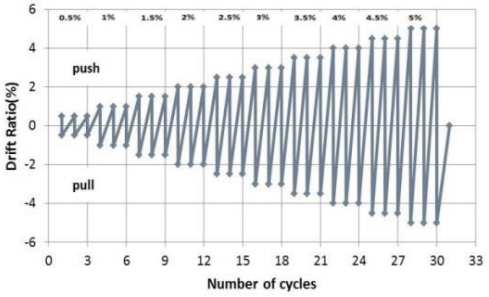

Figure 11. The cyclic loading pattern

3- Test results

3- 1- Load-story drift

In Figure 12, the specimens' force-drift curves of the beam ends are shown. The drift is presented in terms of percentages. Clearly, the stiffness and strength of the specimens 1 to 4 has changed in each hysteresis loop of each load cycle. At a specific drift, the load applied to the beam end has reached its maximum value, and it has been reduced in the next cycles. It is worthwhile to highlight that the load carrying capacity of the specimens was about 30 kN and it was achieved at the drifts ranged from 2% to 3%. By comparing the hysteresis loop, it can be observed that the confined specimen made of

high-strength concrete was slightly pinched (Specimen 3). For the unconfined specimen with the low strength concrete, the significant pinching occurs (Specimen 2). In Figure 13, beam end drift curves of the specimens reinforced with the GFRP bars are shown. In specimens 5 to 8, the stiffness and strength have been slightly changed in each cycle. However, at a specific drift, the load applied to the beam end has reached its maximum value, and it has gradually reduced in the next cycles. The load carrying capacities of all the specimens were ranged between 15 kN to 25 kN and it was achieved at the drifts ranged from 2% to 3%. By comparing the hysteresis loops, it can be observed that specimen 7 which was confined and made of high-strength concrete was slightly pinched. For specimen 6, unconfined and made of the low strength concrete, the significant pinching occurred.

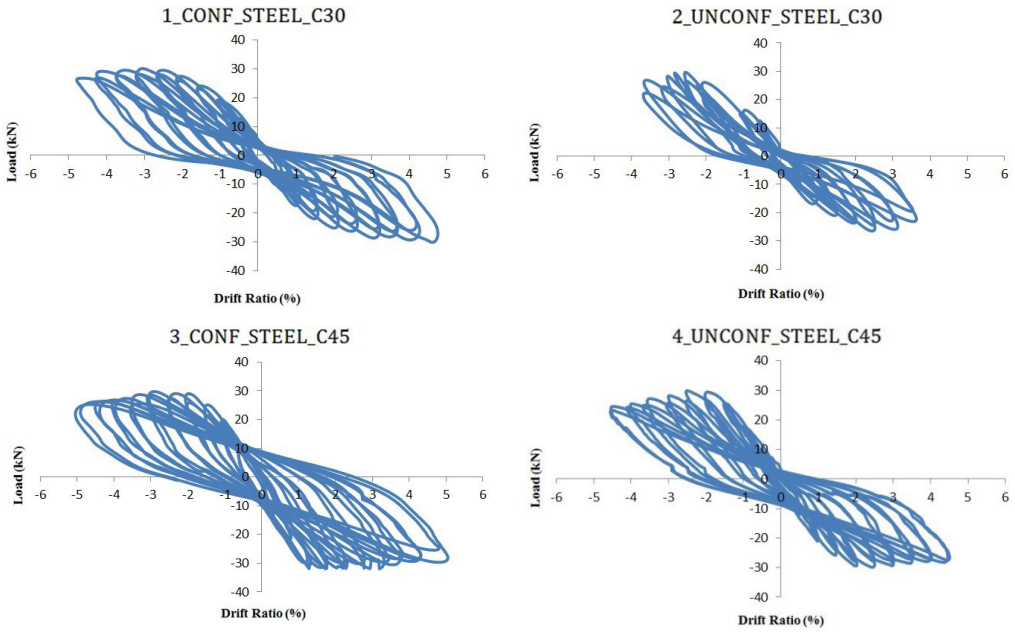

Figure 12. Load-story drift curve of the beam tip in steel bars specimens

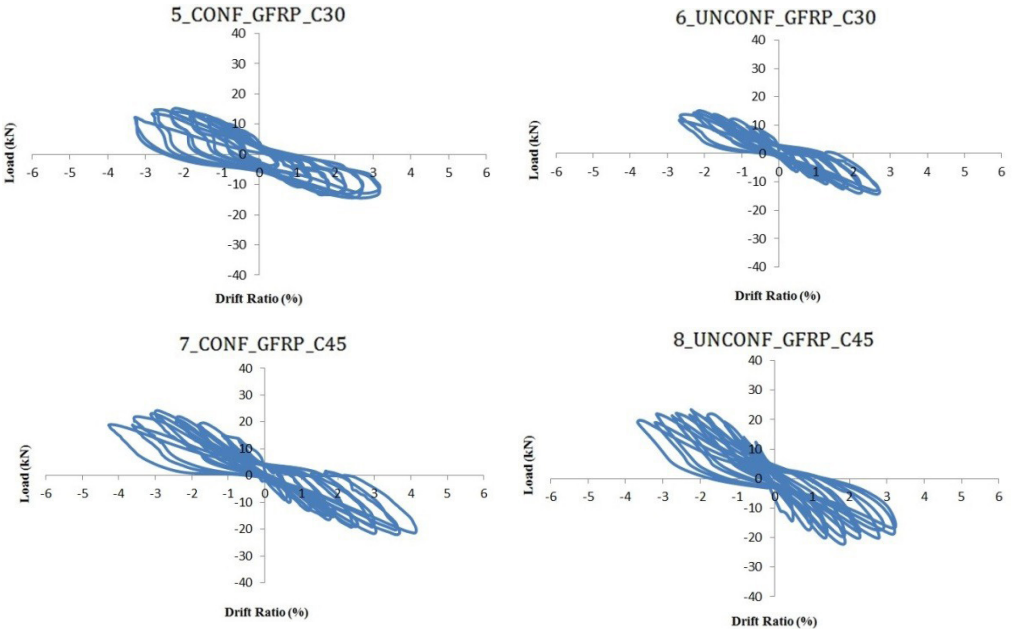

Figure 13. Load-story drift curve of the beam tip in GFRP bars specimens

3- 2- Load-story drift envelope

By connecting the maximum story drift points corresponding to each displacement level, the load-story drift envelope curve is obtained. In Figure 14a and b, the load-story drift envelope curve of the specimens reinforced with steel and FRF are illustrated. ACI Committee [33] suggested provisions for a connection to be accepted as an element of a moment resistant frame in seismic regions. Based on this code, in the third cycle in which the drift of 3.5% is obtained, the maximum applied load in each loading direction should not be less than 75% of the maximum lateral strength in the aforesaid direction to satisfy the fracture criterion. Moreover, the observed energy ratio should not be less than 0.125, and the secant stiffness about zero (the secant stiffness corresponding to the drifts ranged from -0.35% to 0.35%) should not be less than 5% of the initial stiffness at the first cycle of the aforesaid direction. Based on Figures 14a and b and the requirements of ACI Committee [33], the seismic behavior of the specimens were assessed. Accordingly, the behavior of the specimens reinforced with the steel bars is acceptable. Moreover, the specimens reinforced with the FRP bars satisfied the acceptance criteria of ACI Committee [33], and the behavior of the specimen 7 and 8 with high strength concrete were acceptable as well. Note that; the specimens 5 and 6 did not satisfy the criteria of the 3.5% drift. Hence, they could not be accepted. According to Corley's suggestions [25], the performance of specimens 5 and 6 was not satisfactory. Corley [25] suggested the third cycle in which the drift of 3% was occurred for satisfying the fracture criterion. In this displacement, the connection behavior ought to be stable. Specimens 5 and 6 were not able to reach the drift of 3% although the behavior of specimen 5 was stable in drifts beyond 3% due to the compressive forces. Based on the load-story drift envelope curves, usage of GFRP bars in connection showed an acceptable drift capacity, assuming a minimum drift demand of 3% as suggested in the literature for ductile frame structures [25].

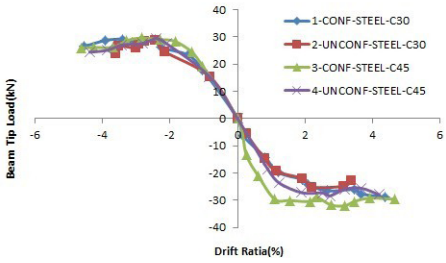

(a) steel

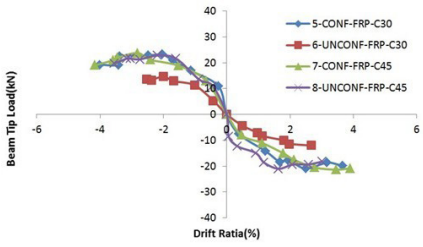

(b) GFRP

Figure 14. Load-story drift envelope of specimens

3- 3- Cracking patterns

At the drift of 5%, the cracking patterns of the specimens reinforced with steel and GFRP bars are shown in Figure 15 and 16, respectively. Based on Figure 15, the shear fracture occurred in the connection core of specimens 1 and 2. It should be reminded that specimen 1 was confined and made of the low strength concrete, and the specimen 2 was unconfined. It is worthwhile to mention that the flexural fracture occurred outside the connection zone of the confined and unconfined specimens (specimens 3 and 4) made of high-strength concrete. The crack width in the confined specimens made of low and high strength concrete (specimens 1 and 3) was less than that of the unconfined ones (specimens 2 and 4). The drift value in lieu of displacements of 31.5, 36 and 40.5 mm are 3.5%, 4% and 4.5%, respectively. In beam-column connections reinforced with steel bars, the shear fracture occurred in the connection core. But, increasing the confinement level and concrete strength resulted in flexural fracture outside the connection core of these specimens.

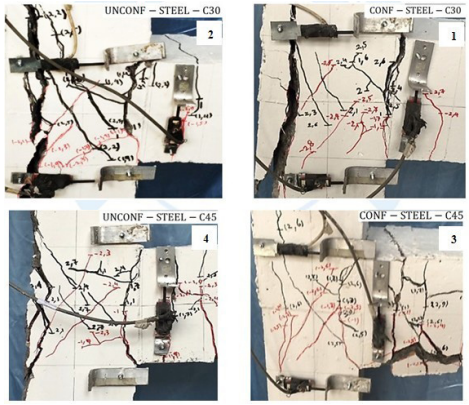

Figure 15. The cracking patterns of specimens reinforced with steel bars

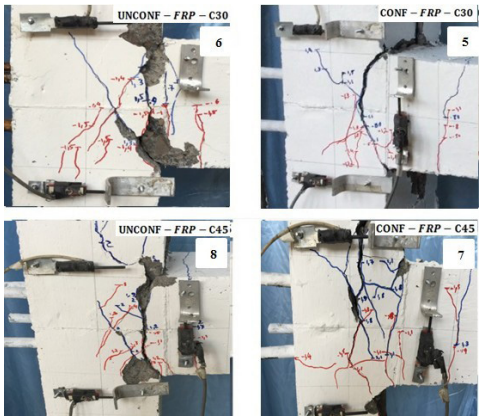

Figure 16. The cracking patterns of specimens reinforced with GFRP bars

Based on Figure 16, in the specimens reinforced with GFRP bars, the hairline crack was occurred in the first steps of loading and at the initial displacements. After reaching to greater displacements, the crack width increased, and

continued to spread from the beam-column connection. In specimens 6 and 8 made of low and high strength concrete, the cracks continued to propagate from the beam-column connection, and by increasing the cyclic load, some parts of the beam-column connection under pressure crunched and were separated from the section. Similarly, at the displacements greater than 35 mm, the concrete cover separation occurred at the beam-column connection. In specimen 5 and 7 which were made of low or high strength concrete, increasing the confinement level led to reduction in the crack width. However, the cracks continued to spread at the connection despite the fact that the concrete cover separation did not occur at the displacements greater than 40 mm. In specimens reinforced with GFRP bars and made of low or high strength concrete, the cracks in the connection core were negligible, and the cyclic loading closed them. By increasing the applied load, the flexural fracture occurred in the beam-column connection. Moreover, increasing the confinement level reduced the crack width, and prevented the occurrence of the cover separation.

3- 4- Energy Dissipation

The ability of energy dissipation is one of the key factors in designing the structures. The more a structure is able to dissipate energy, the higher its chance gets to stay stable during an earthquake. It should be noted that increasing the confinement level and concrete strength results in more energy dissipation and less pinching effect [34]. In Figures 17a and b, the accumulative dissipated energy versus the drift is plotted for the specimens reinforced with steel and GFRP bars, respectively. Since the area of the hysteresis loops of the specimens reinforced with the steel bars is greater than that of the specimens with GFRP bars, they can dissipate more than twice of the energy dissipated by the specimens with GFRP bars.

Specimen 2 significantly pinched in the load cycles and the area of its hysteresis loops were less than other specimens. Additionally, the ability of this specimen in energy dissipation was less than other specimens. As previously mentioned increasing the concrete strength can improve the hysteresis loops and increase the energy dissipation ability. Consequently, the maximum energy dissipation occurred in specimen 3. With regard to the energy dissipation ability, the behavior of specimens reinforced with GFRP is similar to the specimens with steel reinforcement, but the specimens with steel bars can dissipate more energy relative to the specimens reinforced with GFRP. In specimen 5 and 8, the maximum energy dissipation occurs by reaching the drift of 3%, but the maximum energy dissipation of specimens 6 and7 occurred before reaching to the drift of 2% and 4%, respectively. In case of specimens with GFRP bars, increasing the confinement level improve the energy dissipation ability. A reduction of 34% was observed in the energy dissipation of the confined specimens with GFRP bars and high strength concrete in comparison to the corresponding specimens reinforced with steel bars. Moreover, the energy dissipation of the confined specimens with GFRP bars and low strength concrete was reduced by 26%, in comparison to the corresponding specimens reinforced with steel bars. Although the energy dissipation ability of specimens with GFRP bars is less than that of specimens with the steel one.

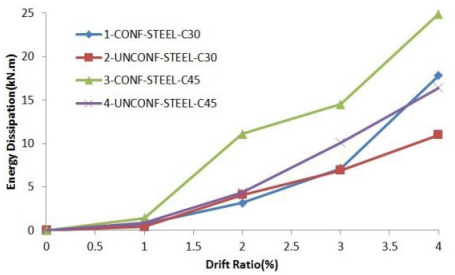

(a) steel

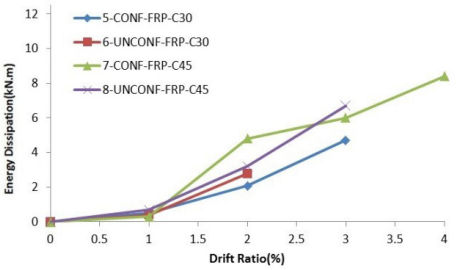

(b) GFRP

Figure 17. The amount of dissipated energy versus the drift for the specimens

3- 5- Secant stiffness relationship

Secant stiffness is measured as the peak-to-peak stiffness of the beam tip load-story drift relationship. It is computed as the slope of the line joining the peak of positive and negative loads at each load cycle. The secant stiffness is an indicator of the response of the specimen during a load cycle and its strength degradation from one cycle to the next cycle. Loss of stiffness of reinforced concrete elements during cyclic loading is due several internal damage mechanisms [35]. In Figures 18a and b, the secant stiffness relationship versus the drift is plotted for the specimens reinforced with steel and GFRP bars, respectively.

The steel-reinforced specimens had a loss of stiffness led to damage in the beam plastic hinge zone higher initial stiffness. The maximum drift achieved was 5.0% and 4.0% for specimens 1, 3, 4 and specimen 2 with steel bars, respectively. The GFRP specimens had negligible reduction in stiffness after 2% story drift, which were relate to the consolidation of cracks and the limited damage to concrete. The maximum drift achieved was 4% and 2.5% for specimens 7, 8 and specimen 6 with GFRP bars, respectively. An examination of the plots indicated that the specimen 3 with steel bars and the specimen 7 with GFRP bars had higher initial stiffness.

By increasing concrete strength in confined and unconfined for steel bars (specimens 3 and 4) had higher stiffness. Stiffness in confined and unconfined specimens with high strength concrete for steel bars (specimens 3 and 4) had higher than that of confined and unconfined specimens with low strength concrete (specimens 1 and 2). By increasing concrete strength in confined specimens for GFRP bars (specimens 5 and 7) had higher stiffness. Stiffness in confined specimens with low and high strength concrete for GFRP bars (specimens 5 and 7) had higher than that of unconfined specimens (specimens 6 and 8).

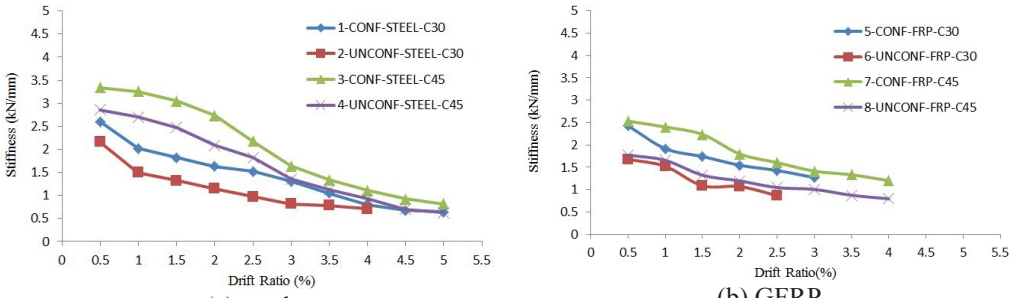

(a) steel (b) GFRP

Figure 18. The amount of secant stiffness versus the drift for the specimens

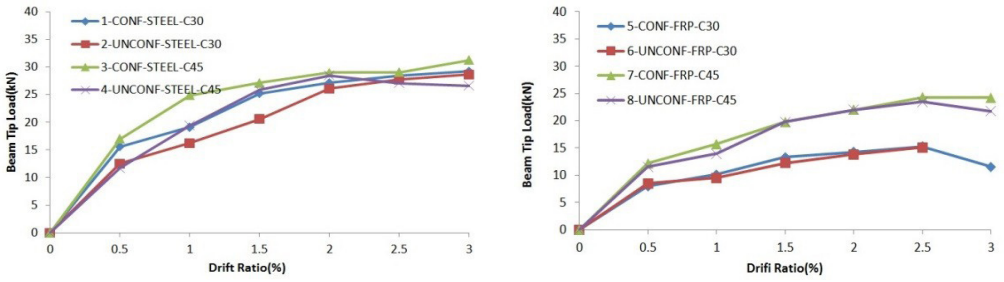

(a) steel (b) GFRP

Figure 19. The envelope of the load applied at the beam tip load for the specimens

Stiffness in confined specimens with low and high strength concrete (specimens 1 and 3 for steel bars and specimen 5 and 7 for GFRP bars) is smaller than that of unconfined specimens (specimens 2 and 4 for steel bars and specimen 6 and 8 for GFRP bars), respectively.

3- 6- The load applied to the beam tip load envelop

For all specimens, the envelope of the load applied to the beam tip load is presented in Figures 19a and b. For the specimens reinforced with steel bars, the initial stiffness is more than that of specimens reinforced with GFRP bars. In specimens with steel bars, the force increment is considerable before reaching the drift of 2%. After this drift, the load increment is negligible. The behavior of specimens 5 and 6 with GFRP bars are similar. Furthermore, the behavior of specimens 7 and 8 are analogous. Prior to reaching the drift of 2.5%, the load was considerably increased. After this step, the load increment is ignorable. Although all the properties of the specimens such as the cross-sectional areas of the steel and GFRP are the same, the measured force at the end of the beam reinforced with steel is more than those with GFRP bars. In comparison to specimens 5 and 6 reinforced with GFRP bars, the increment of 50% can be observed in the maximum load increment of the specimens 1 and 2 is 50%. Furthermore, the maximum load increment of specimens 3 and 4 reinforced with steel bars has increased by 20%, in comparison to the specimens 7 and 8 reinforced with GFRP bars.

3- 7- Moment-Curvature Curves

By using the moment-curvature curve, the non-linear flexural properties of a reinforced concrete section can be assessed. Due to the fact that the location of the neutral axis and the load carrying capacity are not constant in the element length, the curvature changes along the element length. As described in Section 2-3 and presented Figuress. 8 and 9, the vertical displacement of the beam Δ_2 in the critical zone was measured by LVDT2. Moreover, the vertical displacementsΔ_5, as well as the horizontal displacements Δ_3 and Δ_4 were measured by LVDT5, LVDT3 and LVDT4, respectively. θ_c is the rotation of the connection node measured by LVDT2 and LVDT5 and Δ is displacement measured by LVDT2 and LVDT5 using Equations. (2) and Eq. (3). L is the distance between two horizontal LVDTs (3 and 4) installed on the column that is 300 mm for all specimens. The displacement of the beam at the distance of 2h from the column face is presented by Δ_{Beam}, and it can be calculated by Equation. (4). In this equation, h (beam height) is assumed to be 200 mm [36].

Assuming that the deformed shape of the critical zone of the beam is circle arc whose radius is R, the curvature of the beam (1/R) can be computed, based on the geometry of the presumed deformed shape and the principles of the strength of materials. R can be obtained with the help of Equation. (5). The deformed shape of the beam is illustrated in Figure. 20.

$$(\Delta_{Beam} - R)^2 + X_0^2 = R^2 \quad (1)$$

$$\theta_c = (\Delta_4 - \Delta_3)/L \quad (2)$$

$$\Delta = \Delta_2 - \Delta_5 \quad (3)$$

$$\Delta_{Beam} = \Delta - \theta_c \times 2h \quad (4)$$

$$R = \frac{\Delta_{Beam}^2 + X_0^2}{2\Delta_{Beam}} \quad (5)$$

$$\varphi = \frac{1}{R} \quad (6)$$

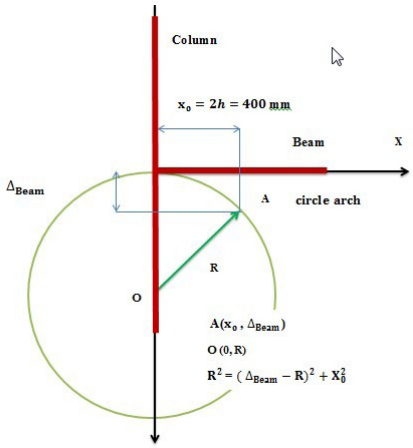

Figure. 20. The deformation of the beam-column connection [36]

In Figure. 20, x_o represent the beam lateral displacement (the location of LVDT2), and it is equal to 400 mm. The parameter φ is the beam curvature. By using the equations Equations (1) to (6), the moment-curvature curve of specimens reinforced with steel and GFRP bars are shown in Figure. 21 and Fig. 21, respectively.

Based on Figure. 21, it is obvious that the moment-curvature curve of specimens 1-4 is linearly extended until reaching to the yield point of the steel bars. Clearly, yielding of steel leads to an increment in the curvature, but it does not considerably affect the moment. In these specimens, the curvature of the beams did not play an important role, and the curves of all specimens are similar prior to reaching the moment of 14 kN-m. Note that; the curvature of the specimen 1 is greater than specimen 2 due to its confinement. It should be reminded that the strength and confinement level of specimen 3 was greater than other specimens. For this reason, its curvature is greater than other specimens. In Figure. 21, the linear behavior of specimens 5 to 8, reinforced with GFRP bars, are illustrated. Before the occurrence of curvature of 1%, the behavior of all specimens is the same. After reaching to this degree of curvature, the moment and curvature simultaneously increases. In these specimens, the moment is less than that of specimens reinforced with steel bars. In all specimens (except for specimen 7), the curves are similar before reaching to moment of 4 kN.m. As a result of confinement of specimens 5 and 7, their curvature is greater than that of specimens 6 and 8. It should be reminded that the strength and confinement of specimen 7 is more than other specimens.

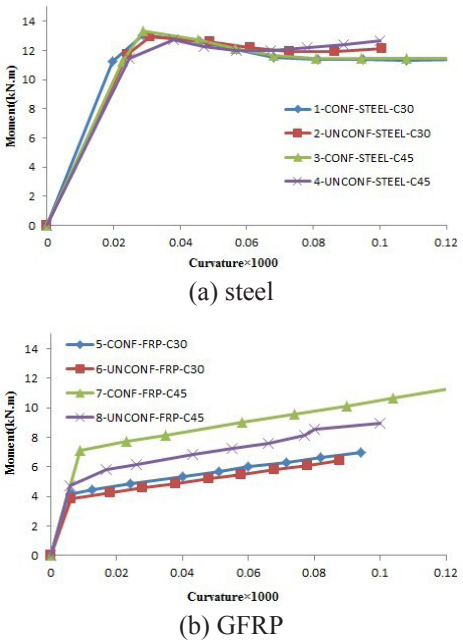

Figure 21. Moment-curvature curve for the specimens

4- The finite element analysis

In this section, the concrete connection under the cyclic loading is analyzed with the help of Seismo-Struct commercial software. This software is able to assess the material and geometric non-linear behavior of the frames under static and dynamic loads. Additionally, it can model various materials such as: concrete, steel, FRP and SMA [37].

4- 1- Modeling the concrete materials

In this software, the concrete behavior can be modeled using different models whose stress-strain relationships are not similar. One of these models was proposed by Mander et al. [38], and it is a non-linear uniaxial model which considers the constant confinement level. In Figure. 22, the stress-strain relationship of the confined and unconfined concrete under cyclic loading is shown.

In this model $f_c^{'}$ is the compressive stress of the concrete acquired using Equation. (7). This equation includes the increasing and decreasing branches of the stress-strain curve. The parameters utilized in this equation can be calculated by utilizing equations 8 to 9 [37].

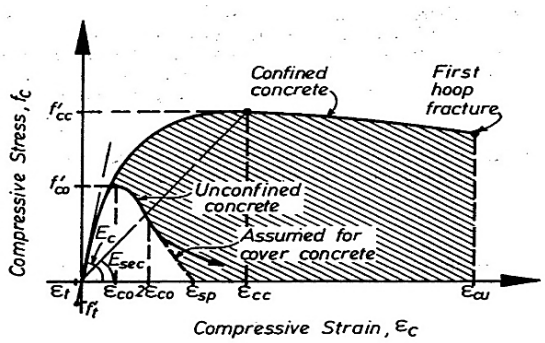

Figure 22. The stress-strain curve of the confined and unconfined concrete under cyclic loading [37].

$$f'_c = \frac{f'_{cc} x r}{r - 1 + x^r} \quad (7)$$

$$x = \frac{\varepsilon_{co}}{\varepsilon_{cc}}, f'_{cc} = k f'_{co}, \varepsilon_{cc} = \varepsilon_{co}\left[1 + 5\left(\frac{f'_{cc}}{f'_{co}} - 1\right)\right] \quad (8)$$

$$E_c = 5000\sqrt{f'_{co}}, E_{sec} = \frac{f'_{co}}{\varepsilon_{cc}}, r = \frac{E_c}{E_c - E_{sec}} \quad (9)$$

In these equations, $f_c o'$ and f'_{cc} denote to the strength of the confined and unconfined concrete, respectively. Moreover, K is equal to the ratio of the confined concrete strength to the strength of the unconfined concrete, and ε_{cc} is the compressive strain along specimen length in the confined concrete, ε_{co} is the strain corresponding to the strength of unconfined concrete and r is the modulus of elasticity ratio.

Moreover, the elasticity modulus of the concrete and its secant elasticity modulus are presented by Ec and Esec, respectively. In SeismoStruct software, the tensile strength f_t represents the tensile stress capacity of the material, and it is estimated by $K_t=\sqrt{(f_c')}\times f_t$ in which kt is between 0.5 and 0.75. Note that; K_t is 0.5 for concrete under direct tension, and it is equal to 0.75 for concrete subjected bending load. The values of these parameters were presented by Mander et al [38]. In this software, the default value of this parameter is 24 kN/m^3.

4- 2- Modeling bars

For modeling the specimens reinforced with FRP bars, Trilinear FRP model has been employed [37]. In Figure. 23, this model is shown. The stress-strain curve of this model includes three lines, and it is uniaxial model in which there no resistance against compression. In this model, four parameters are used to define the mechanical properties. They are presented by E_1 ,E_2 ,γ ,f_t is the ultimate tensile strength, and it is assumed to be 0.8 GPa. Moreover, the bars density is shown by γ, and it is equal to 1.8E-5 N/mm^3. Furthermore, E_1 is the initial stiffness which is 43 GPa. The secondary stiffness is shown by E_2, and it is equal to 500 GPa. The values of these parameters have been determined based on the experimental results.

In these specimens, Monti-Nuti model is applied for the columns, and the Menegotto-Pinto model is utilized for the beams and columns reinforced with steel bar [37]. The suggested stress-strain equations of this model related to the hardening isotropic rule were proposed by Filippou et al. [39]. According to the research conducted by Prota et al [40], the application of this model is limited to the reinforced concrete structures under complicated loading patterns, and they may experience considerable load return. Herein, the Poisson's ratio and elasticity modulus of steel are assumed to be 0.3 and 200000 MPa, respectively.

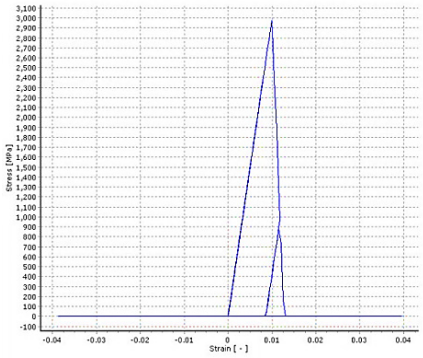

Figure 23. The trilinear model (FRP bars) [37]

4- 3- The geometry modeling and structural analysis

In this work, beams and columns have been divided into 2 and 4 elements, respectively. For analyzing the connections, the static time history analysis was performed. In SeismoStruct software, the elements' properties are defined in the element classes module. For modeling the frame elements, inelastic force-based plastic hinge frame element type (infrmFBP) was used. In modeling process, various elements with different properties were employed. After defining the elements' properties, the element connectivity module was applied for connecting the elements.

It should be added that the geometry model of the structure was created in three steps. At the first stage, all the structural and non-structural nodes were defined. Then, the method of connecting elements was specified. Finally, the restraints related to the structural boundary conditions were assigned. In Module of supports, the boundary conditions were introduced. In this module, all the structural nodes are listed, and it is possible to restrain all the degrees freedom of the structure [37]. The finite element model of the specimens is presented in Figure 24. Additionally, in Figures 24, the connection modeling, the elements' properties and the characteristics of the nodes are illustrated.

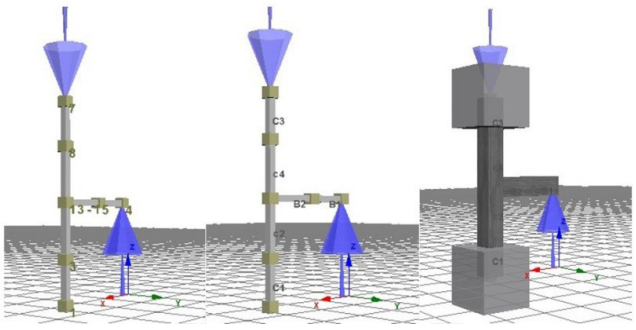

a. connection modeling b. Elements' properties c. Nodes' properties

Figure 24. The finite element of the specimens

4- 4- Results of analysis

In Figures 25 and 26, the numerical results are compared with the experimental load-story drift curves of the beam end of the specimens reinforced with steel and GFRP bars. Based on Figure 25, in specimens reinforced with steel bars and made of low strength concrete, a considerable pinching effect is observed (specimen1 and 2). The experimental and

analytical results of the confined specimens made of high strength concrete are more compatible, in comparison to other specimens (specimen 3). According to Figure 26, in the specimens reinforced with GFRP bars, the pinching effect is observed. In specimens made of high strength concrete, the pinching effect in load-story drift loops is less than other specimens, due to the fact the connection compressive strength are greater than other specimens (specimens 7 and 8).

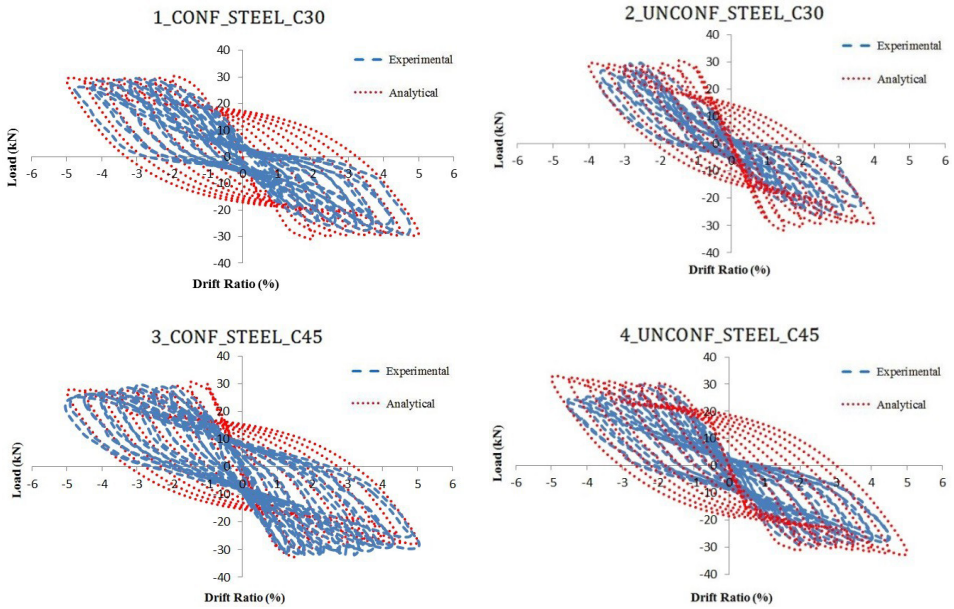

Figure 25. Comparison of analytical and experimental results of the beam tip load-story drift curve in steel bar specimens

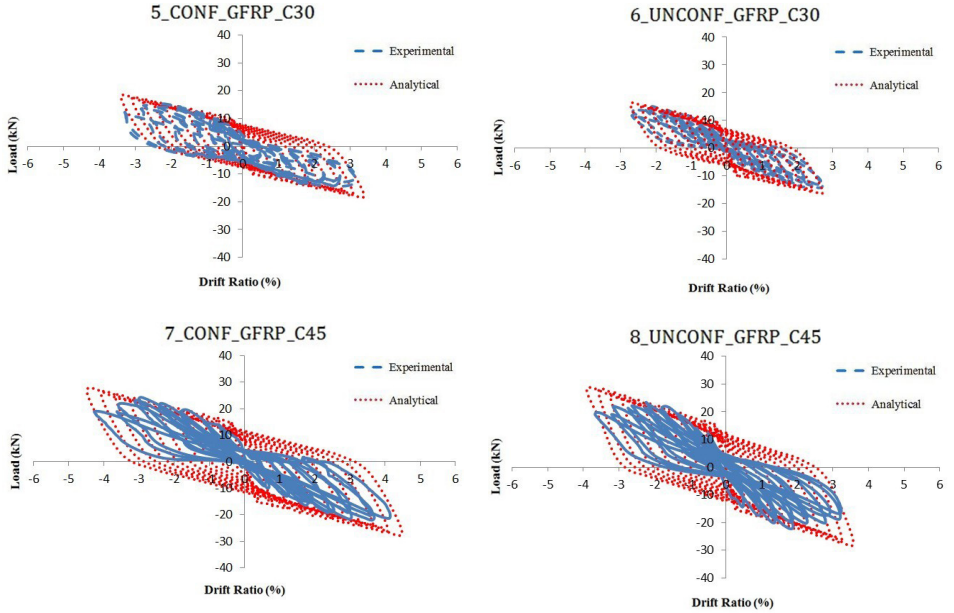

Figure 26. Comparison of analytical and experimental results of the beam tip load-story drift curve in GFRP bar specimens

5- Conclusion

In this paper, the behavior of the connections reinforced with the GFRP and steel bars under cyclic loading was experimentally assessed. For this purpose, 8 beam-column connections with GFRP and steel bars were constructed. The compressive strength of the concrete adopted for these specimens were not similar. The behavior of the specimens was also analyzed by SeismoStruct software. Based on the results of the study, the following conclusions are drawn:

- In specimens reinforced with GFRP bars and made of low or high strength concrete, the crack in the connection core were negligible, and the cyclic loading closed them.

By increasing the applied load, the flexural fracture occurred in the beam-column connections. Moreover, increasing the confinement level reduced the crack width, and prevented the occurrence of the cover separation. In beam-column connections reinforced with steel bars, the shear fracture occurred in the connection core. Increasing the confinement level and concrete strength resulted in flexural fracture outside the connection core of these specimens.

- The GFRP-reinforced beam-column connection showed an elastic behavior with very low plasticity features under cyclic loading. This resulted in lower energy dissipation compared to the steel-reinforced beam-column connections.
- The GFRP-reinforced beam-column connections showed lower stiffness than that of the steel-reinforced beam-column connections. By increasing concrete strength in confined specimens for GFRP bars had higher stiffness. Stiffness in confined specimens with low and high strength concrete for GFRP bars had higher than that of unconfined specimens.
- Based on the load-story drift envelope curves, usage of GFRP bars in connection showed an acceptable drift capacity, assuming a minimum drift demand of 3% as suggested in the literature for ductile frame structures.
- Specimens were analyzed by SeismoStruct finite element software. Comparison between analytical and experimental results of the beam tip load-story drift curve showed a good correlation in all specimens.

References

[1] R.L. Park, R. Park, T. Paulay, Reinforced concrete structures, John Wiley & Sons, 1975.

[2] T. Paulay, M.J.N. Priestley, Seismic design of reinforced concrete and masonry buildings, (1992).

[3] A.M. Said, Investigation of Reinforced Concrete Beam-column Joints Under Reversed Cyclic Loading, 2005.

[4] T.H.-K. Kang, S.-S. Ha, D.-U.J.A.S.J. Choi, Bar Pullout Tests and Seismic Tests of Small-Headed Bars in Beam-Column Joints, 107(1) (2010).

[5] S. Barbhuiya, A.M.J.E.S. Choudhury, A study on the size effect of RC beam–column connections under cyclic loading, 95 (2015) 1-7.

[6] M. Engindeniz, L.F. Kahn, Z.J.A.s.j. Abdul-Hamid, Repair and strengthening of reinforced concrete beam-column joints: State of the art, 102(2) (2005) 1.

[7] Y. Nakayama, H. Nakai, T. Kanakubo, BOND BEHABIOR BETWEEN DEFORMED ARAMID FIBER-REINFORCED PLASTIC REINFORCEMENT AND CONCRETE, in: The 14th World Conference on Earthquake Engineering October, 2008, pp. 12-17.

[8] A. Said, M.J.A.C.M. Nehdi, Use of FRP for RC frames in seismic zones: Part I. Evaluation of FRP beam-column joint rehabilitation techniques, 11(4) (2004) 205-226.

[9] H.A. Toutanji, M.J.A.s.j. Saafi, Flexural behavior of concrete beams reinforced with glass fiber-reinforced polymer (GFRP) bars, 97(5) (2000) 712-719.

[10] S.R. Salib, G.J.S.J. Abdel-Sayed, Prediction of crack width for fiber-reinforced polymer-reinforced concrete beams, 101(4) (2004) 532-536.

[11] P. Vijay, Aging and design of concrete members reinforced with GFRP bars, (2000).

[12] P.X.J.J.o.c.f.c. Zou, Long-term deflection and cracking behavior of concrete beams prestressed with carbon fiber-reinforced polymer tendons, 7(3) (2003) 187-193.

[13] P.X.J.J.o.c.f.c. Zou, Flexural behavior and deformability of fiber reinforced polymer prestressed concrete beams, 7(4) (2003) 275-284.

[14] P.X.J.J.o.c.f.c. Zou, Theoretical study on short-term and long-term deflections of fiber reinforced polymer prestressed concrete beams, 7(4) (2003) 285-291.

[15] S. Alsayed, Y. Al-Salloum, T. Almusallam, M.J.S.P. Amjad, Concrete columns reinforced by glass fiber reinforced polymer rods, 188 (1999) 103-112.

[16] M. Grira, M. Saatcioglu, Reinforced concrete columns confined with steel or FRP grids, in: Proceedings of the 8th Canadian Conference on Earthquake Engineering, 1999, pp. 445-450.

[17] E.F. Shehata, Fibre-reinforced polymer (FRP) for shear reinforcement in concrete structures, (1999).

[18] T. Nagasaka, H. Fukuyama, M.J.S.p. Tanigaki, Shear performance of concrete beams reinforced with FRP stirrups, 138 (1993) 789-812.

[19] M. Sugita, NEFMAC-Grid type reinforcement, in: Fiber-Reinforced-Plastic (FRP) Reinforcement for Concrete Structures, Elsevier, 1993, pp. 355-385.

[20] E.A. Ahmed, F. Settecasi, B.J.J.o.B.E. Benmokrane, Construction and testing of GFRP steel hybrid-reinforced concrete bridge-deck slabs of sainte-catherine overpass bridges, 19(6) (2014) 04014011.

[21] B. Benmokrane, M. Eisa, S. El-Gamal, D. Thébeau, E.J.C.i. El-Salakawy, Pavement system suiting local conditions, 30(11) (2008) 34-39.

[22] H.M. Mohamed, B.J.J.o.C.f.C. Benmokrane, Design and performance of reinforced concrete water chlorination tank totally reinforced with GFRP bars: Case study, 18(1) (2013) 05013001.

[23] P.K. Dutta, D.M. Bailey, S.W. Tsai, D.W. Jensen, J.R. Hayes Jr, Composite Grids for Reinforcement of Concrete Structures, CONSTRUCTION ENGINEERING RESEARCH LAB (ARMY) CHAMPAIGN IL, 1998.

[24] J. Lemaitre, R. Desmorat, Engineering damage mechanics: ductile, creep, fatigue and brittle failures, Springer Science & Business Media, 2005.

[25] W.J.S.P. Corley, Ductility of Column, Wall, and Beams--How Much is Enough?, 157 (1995) 331-350.

[26] J. Sabzi, M.R.J.C. Esfahani, B. Materials, Effects of tensile steel bars arrangement on concrete cover separation of RC beams strengthened by CFRP sheets, 162 (2018) 470-479.

[27] M.A. Aiello, L.J.J.o.C.f.C. Ombres, Structural performances of concrete beams with hybrid (fiber-reinforced polymer-steel) reinforcements, 6(2) (2002) 133-140.

[28] H.Y. Leung, R.J.S.S. Balendran, Flexural behaviour of concrete beams internally reinforced with GFRP rods and steel rebars, 21(4) (2003) 146-157.

[29] S.M. Alcocer, R. Carranza, D. Perez-Navarrete, R.J.P.j. Martinez, Seismic tests of beam-to-column connections in a precast concrete frame, 47(3) (2002) 70-89.

[30] E.Z. Beydokhty, H.J.L.A.j.o.s. Shariatmadar, structures, Behavior of damaged exterior RC beam-column joints strengthened by CFRP composites, 13(5) (2016) 880-896.

[31] A. Bossio, F. Fabbrocino, G.P. Lignola, A. Prota, G.J.B. Manfredi, Design Oriented Model for the Assessment of T-Shaped Beam-Column Joints in Reinforced Concrete Frames, 7(4) (2017) 118.

[32] J. Moehle, J. Hooper, C. Lubke, NEHRP Seismic Design Technical Brief No. 1-Seismic Design of Reinforced Concrete Special Moment Frames: A Guide for Practicing Engineers, 2008.

[33] A.C. Institute, Acceptance Criteria for Moment Frames Based on Structural Testing and Commentary (ACI 374.1-05), (2005).

[34] M.R. Ehsani, F.J.A.S.J. Alameddine, Design recommendations for type 2 high-strength reinforced concrete connections, 88(3) (1991) 277-291.

[35] M.N. Priestley, F. Seible, G.M. Calvi, G.M. Calvi, Seismic design and retrofit of bridges, John Wiley & Sons, 1996.

[36] H. Rezaee Azariani, M.R. Esfahani, H.J.S. Shariatmadar, C. Structures, Behavior of exterior concrete beam-column joints reinforced with Shape Memory Alloy (SMA) bars, 28 (2018).

[37] S. user Manual, Version 5.0. 1, Pavia, Italy. Seismo-Soft Inc. Supporting Services, (2010).

[38] J. Mander, M. Priestley, R.J.J.o.s.e. Park, Observed stress-strain behavior of confined concrete, 114(8) (1988) 1827-1849.

[39] F.C. Filippou, V.V. Bertero, E.P. Popov, Effects of bond deterioration on hysteretic behavior of reinforced concrete joints, (1983).

[40] A. Prota, F. De Cicco, E.J.J.o.E.E. Cosenza, Cyclic behavior of smooth steel reinforcing bars: experimental analysis and modeling issues, 13(4) (2009) 500-519.

Please cite this article using:

H. Rezaee Azariani, H. Shariatmadar, M. Reza Esfahanir, Exterior concrete beam-column connection reinforced with Glass Fiber Reinforced Polymers (GFRP) bars under cyclic loading, *AUT J. Civil Eng.*, 2(2) (2018) 161-176.

DOI: 10.22060/ajce.2018.14611.5487